Supplementary Document

Small-width wall-attached Coandă jets for flow control

Oussama El Mokkadem, Xintong Chen, Charlene Phan, Jérôme Delva, Pierric Joseph, Antoine Dazin and Francesco Romanò

Univ. Lille, CNRS, ONERA, Arts et Métiers Institute of Technology, Centrale Lille, UMR 9014-LMFL-Laboratoire de Mécanique des Fluides de Lille - Kampé de Fériet, F-59000, Lille, France

1 Numerical Methods and Turbulence Modeling

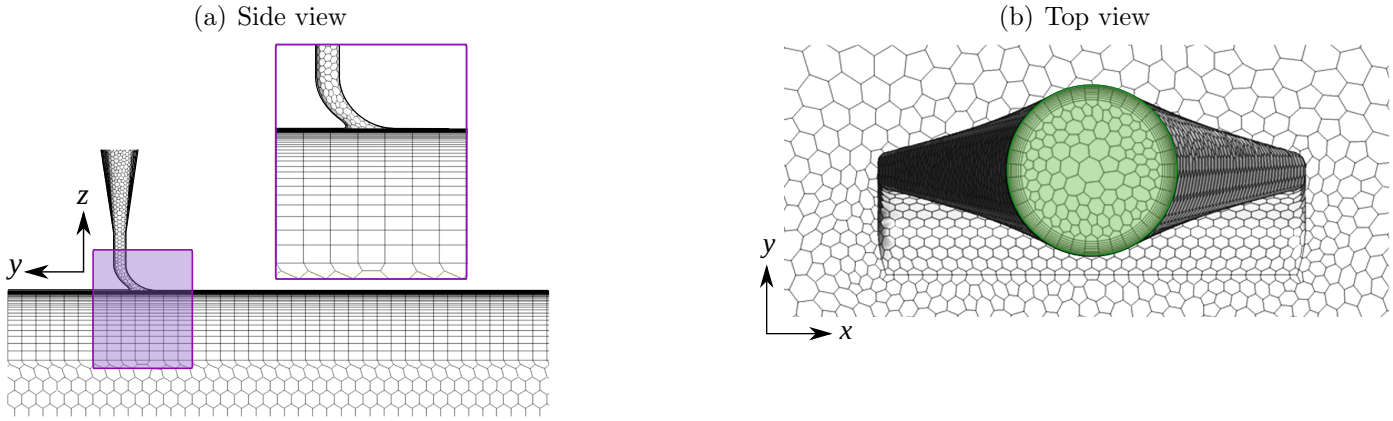

Figure 1: Side (a) and top (b) view of a typical mesh employed for carrying out the three-dimensional URANS simulations in StarCCM+. The depicted mesh has a base size of 1 mm and 40 layers distributed within a distance of 1 mm from the wall. The inset in (a) shows a closeup (violet) of the boundary-layer grid near the plane wall. The green region in (b) denotes the mass-flow inlet.

A typical computational grid used in our StarCCM+ simulations is depicted in fig. 1, where 40 hexahedral layers are distributed within a distance of 1 mm from all the walls. The thickness of such finite volumes is refined with a geometric progression characterized by the stretching factor 1.15. All the StarCCM+ results presented in the paper are obtained using a grid base size of 0.75 mm. For the actuator, the 40-hexahedral-layer refinement is confined within a distance of 1 mm from the inner wall, whereas the refinement at the plane wall distributes 40 hexahedral layers within 5 mm from the $(x, y)-$plane. This distribution is tailored to capture the thin boundary layer inside the actuator and the thicker one attached at the plane wall owing to the Coandă effect. The StarCCM+ grid convergence study leading to the choice of such grid parameters is reported in fig. 2 of the supplementary material and considered four base sizes (i.e. 2, 1, 0.75, and 0.5 mm) and three amounts of hexahedral layers distributed along the injector and flat plate wall (i.e. $N = 10$, 20, and 40 layers). Figure 2 of the supplementary material demonstrates that, if the base size is lower or equal to 0.75 mm, 40 hexahedral layers (total of 1.6M cells) are sufficient to converge on two characteristic velocities of the jet, i.e. the absolute maximum velocity magnitude (top panel) and the relative maximum velocity magnitude on the plane $y/W_\mathrm{n} = -1$ (bottom panel). The base size 0.75 mm and 40 refinement layers have then been selected because they

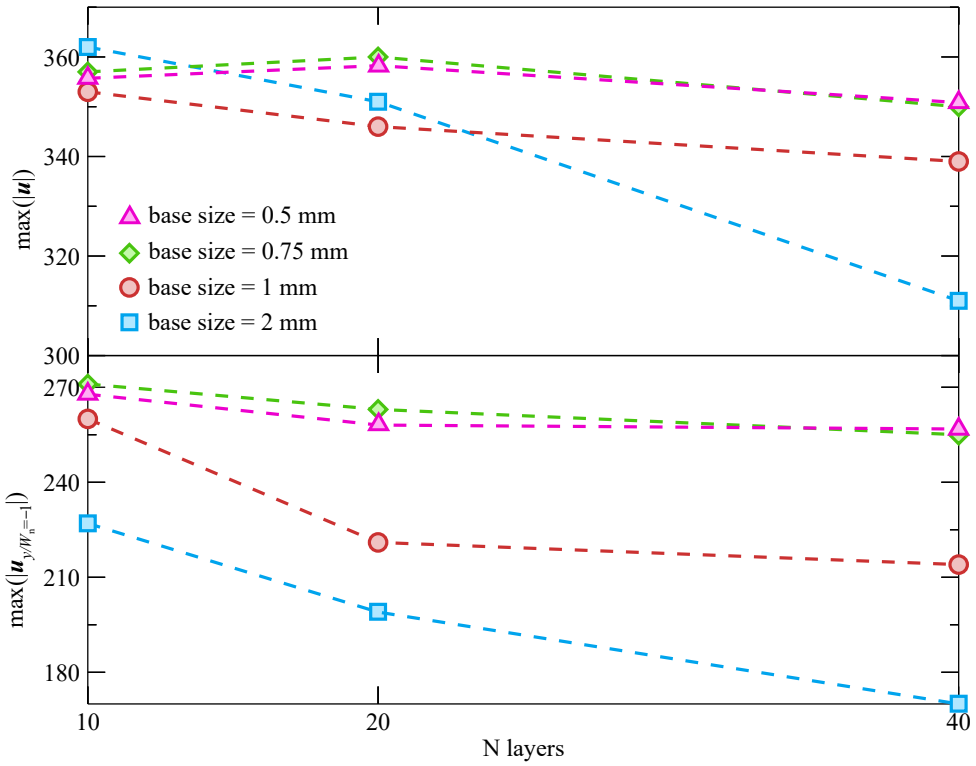

Figure 2: Grid convergence for the StarCCM+ simulations for $\dot{m} = 2$ g/s with $k - \epsilon$, standard, low-Re as turbulence model. The base size and the number of layers near the injector and flat plate walls are varied.

provide mesh converged numerical results with a lower computational effort than if we use 0.5 mm and 40 layers for our grid. All the simulations employ the law of the wall automatically adapted by the software to the selected turbulence model (`wall function` option pre-implemented in StarCCM+). For more details, we refer the reader to the User Guide of StarCCM+ 13.06.012-R8, used to carry out all the StarCCM+ numerical simulations presented in this study.

The unsteady Reynolds averaged Navier–Stokes (URANS) version of the physical model (equation (1) of the paper) employs the `implicit time` discretization option and closes the URANS equation with a turbulence model among the ones already implemented in StarCCM+. A detailed comparative study of the three two-equation models we tested demonstrated that, for the StarCCM+ grid selected in this study, the low-Reynolds and the realizable $k-\varepsilon$ models performed well in reproducing the experimental measurements and the latter has been chosen for simulating all the cases discussed in the paper. The StarCCM+ simulations carried out using the $k - \omega$ SST model presented several criticalities inducing an unphysical mesh-dependent boundary layer separation at the exit of the actuator when grids with a base size of 2, 1, and 0.75 mm have been employed, keeping fixed the parameters that characterize the hexahedral mesh at the walls.

The rationale behind cross-checking our StarCCM+ and OpenFOAM simulations aimed to demonstrate the robustness of our numerical results, regardless of the solver employed, the numerical (converged) grid, and the turbulence model. The mesh used for the OpenFOAM simulations is a 2.5M-cells structured hexahedral grid generated using the tool `blockMesh`. This allows building a mesh that can more finely be tailored to control the y^+ at the injector walls. Figure 3 of the supplementary material shows the grid employed to carry out all the simulations in OpenFOAM. As a result, the OpenFOAM simulations were carried out using the $k - \omega$ SST model of Menter (2003) and employing the standard

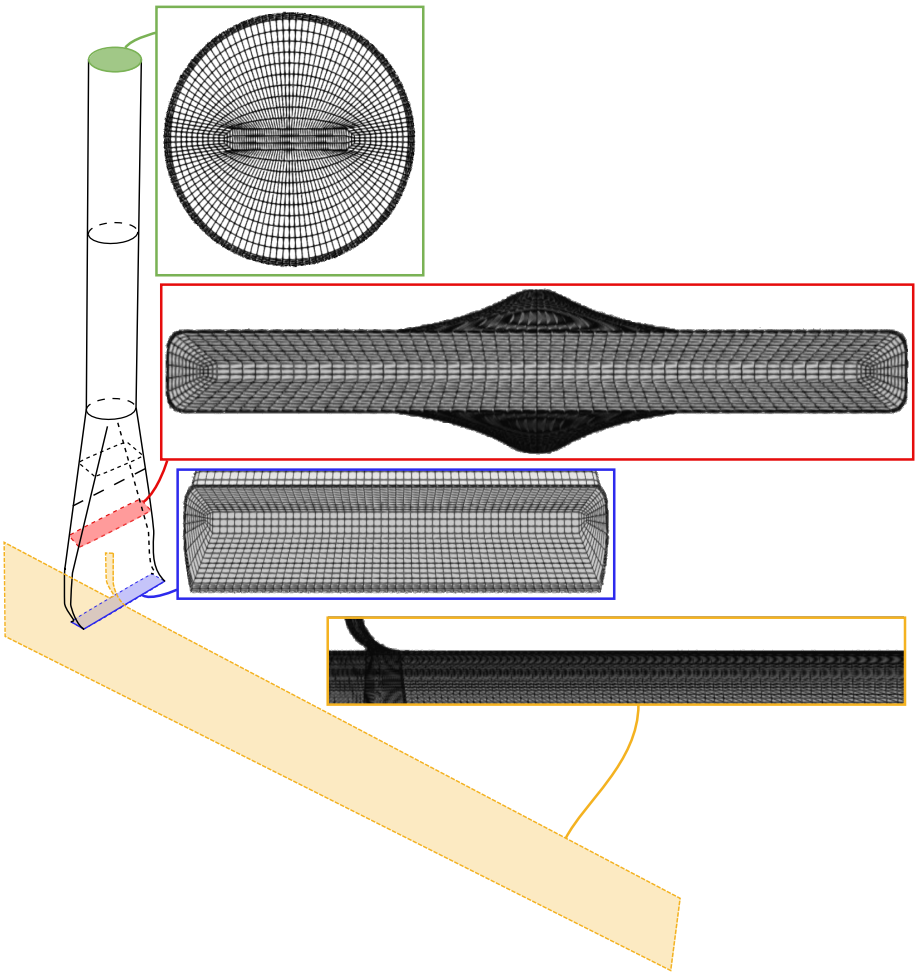

Figure 3: Structured 2.5M-cells OpenFOAM grid meshed using `blockMesh`.

wall function treatment as boundary conditions for all walls. None of such simulations showed numerical artifacts as the grid-dependent separation observed in StarCCM+. Our OpenFOAM $k-\omega$ SST simulations compare well with the corresponding StarCCM+ $k-\epsilon$ standard low-Re simulations, as well as with the experiments (see figs. 4 and 5 of the paper). This demonstrates that the parameters of the turbulence model do not significantly affect the simulation results, provided that the applicability range of y^+ is respected for the tested turbulence models.

2 Experimental Method and Measurements

The jet produced by the actuators has been experimentally investigated in quiescent air. A motorized, three-axes, hot-wire probe carrier was used to determine the velocity field produced by an actuator supplied by an auxiliary pressurized air system. A single-component probe (Dantec 55P11) is used to measure the jet velocity at various locations. Precise positioning of the probe is realized thanks to the camera, leading to an absolute error of less than 0.02 mm in the probe location. The sensing element of the probe is a platinum-plated wire with a 5 μm diameter, 1.25 mm length, and the system relies on a Dantec MiniCTA anemometer. A calibration is realized before each test series for velocities up to 300 m/s. Velocity–time series of 4×10^4 samples are recorded with an acquisition frequency of 20 kHz. Manufacturer data indicates an uncertainty of $\pm$ 1%. In the paper, a single-component probe was used. Hence, only the magnitude of the velocity is presented.

3 Supplementary Results

3.1 Effect of Domain Size and Side-by-Side Injector Interactions

To test the sensitivity of our results to the domain size chosen for our simulations, as well as to the presence of a side injector, we carried out additional simulations in OpenFOAM, keeping fixed the numerical resolution and the turbulence parameters, and varying the sole geometry. At first, we tested the sensitivity of the flow to the size of the domain by setting $W = 20W_n$ and we did not see any significant difference with respect to the corresponding results presented in the paper. Moreover, we compared the results for two injectors side by side with the single-injector configuration. Also in this case, we do not see any significant difference due to the interaction between the two injectors (see fig. 4 of this supplementary document).

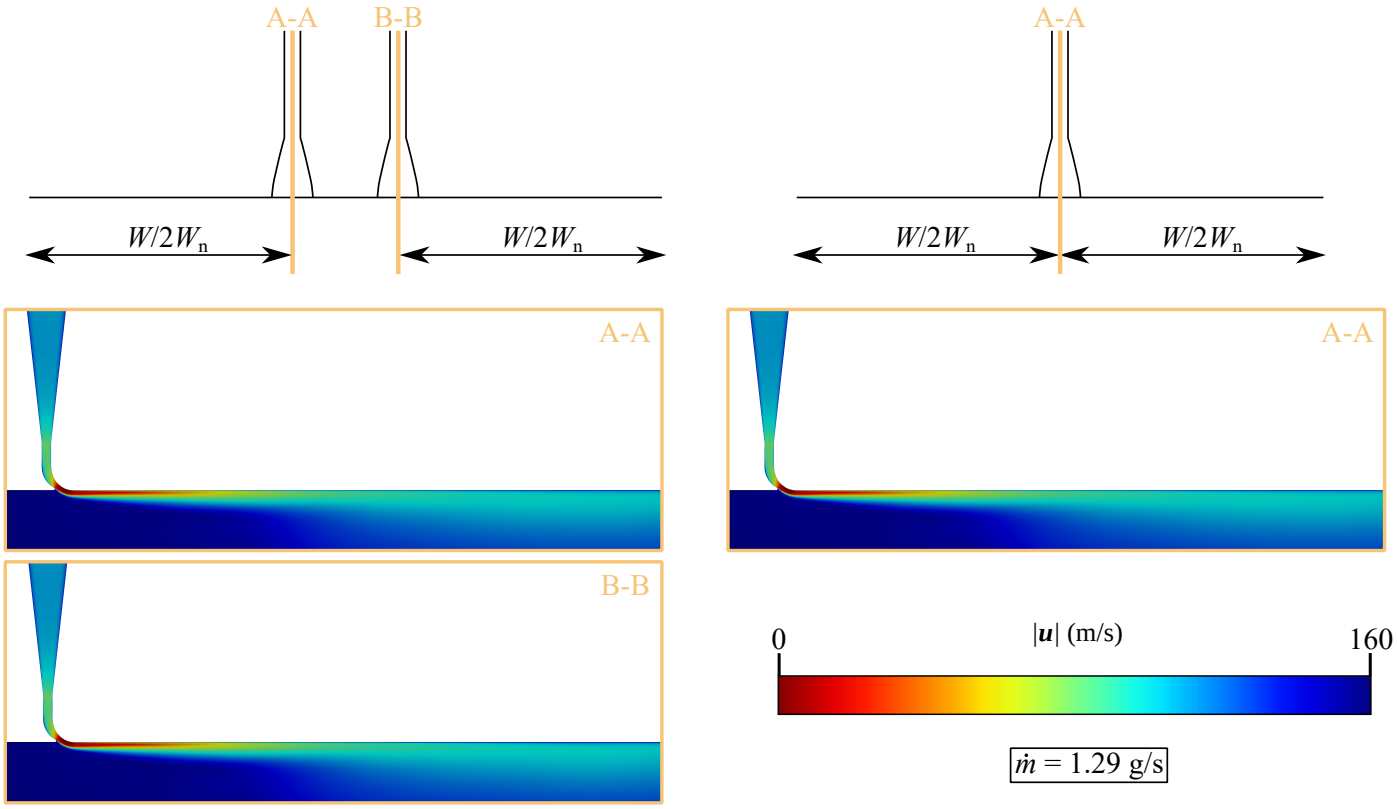

Figure 4: Velocity magnitude for the two- (left) and single-injector (right) configuration for $\dot{m} = 1.29$g/s. The schematics at the top are in scale.

3.2 Effect of Static Pressure, Static Temperature, and Density

Pressure, temperature, and density fields are not discussed in the paper as they are not key to understanding the flow physics specific to the U-shaped wall-attached Coandă jet we investigate. Figure 5 of this supplementary material shows the static temperature field at the top, the static pressure in the middle, and the density field at the bottom. The static temperature field is determined by the convective effects due to the U-shaped jet, i.e. faster regions are cooled down. The static pressure variation is due to the Venturi effect in the injector, and to the Coandă effect right at the outflow of the injector. Except for these two classic features, the static pressure remains almost constant in the rest of the domain, hence it is not affected by the U-shaped jet. Finally, the density results from static

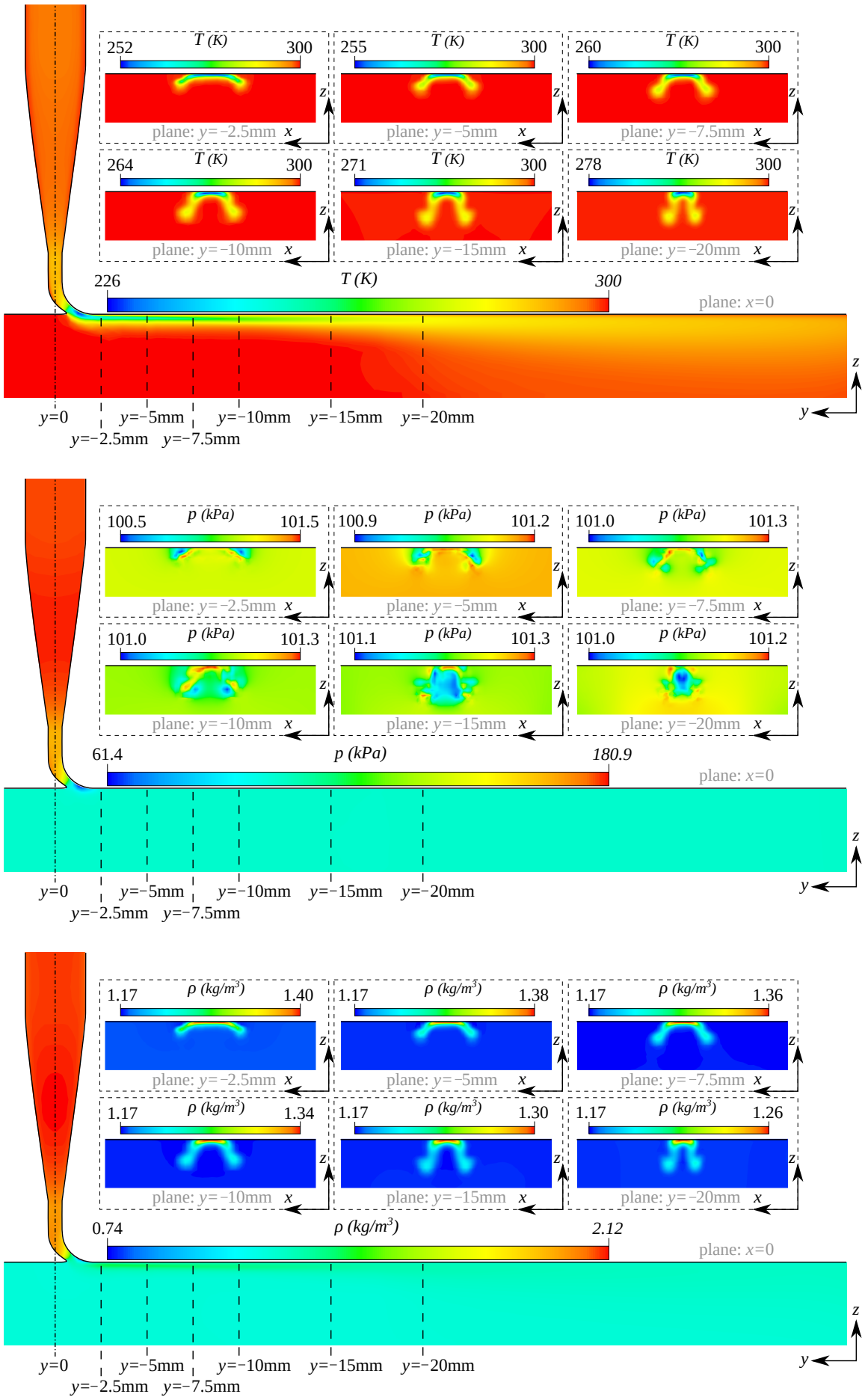

Figure 5: Static temperature T (top), static pressure p (middle), and density ρ (bottom) fields for a single-injector jet on a plane wall for $\dot{m} = 2.15\text{g/s}$.

pressure and temperature owing to the ideal gas constitutive law, and its variations are due to the static pressure inside the injector and the static temperature in the U-shaped jet. The gravitational effects due to density gradients are taken into account, but they do not play a significant role in determining flow physics. Indeed, the effect of buoyancy $\Delta\rho g/\rho(300K) \approx 20m/s^2$ is negligible compared to inertial effects ($|\boldsymbol{u}|^2/W_n \approx (1-10)\times 10^6 m/s^2$).

3.3 Effect of Carter's Curvature

To test the influence of the carter curvature on the flow, one more simulation for the two-injector case is carried out including the curved wall. Figure 6 of this supplementary material demonstrates that the carter curvature does not play any significant role in determining the flow field.

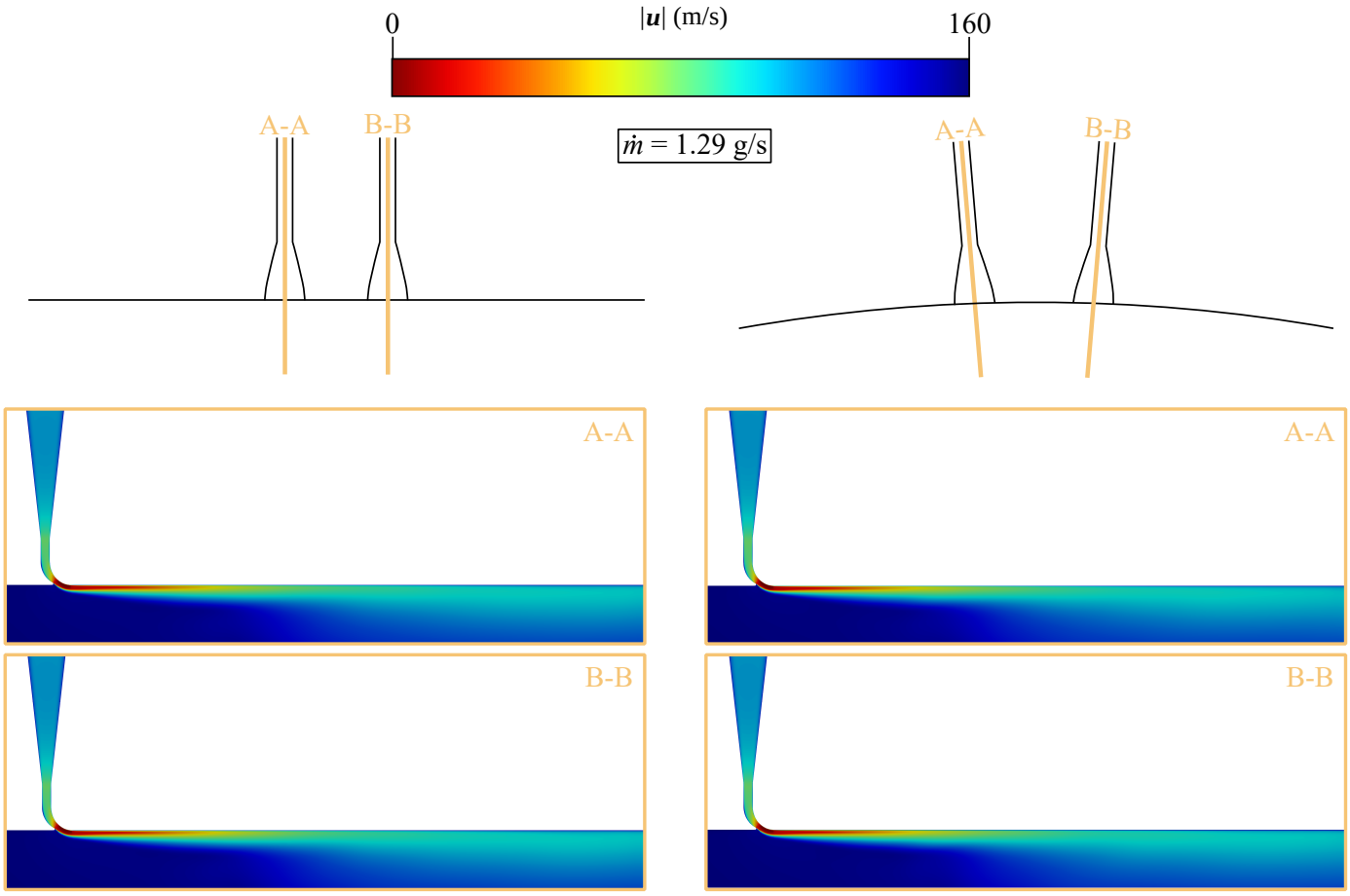

Figure 6: Velocity magnitude for two injectors side by side for $\dot{m} = 1.29$g/s. The figures on the left refer to the plane-wall case, while the figures on the right consider the curved-wall carter with the geometrical parameters derived from CME2. The schematics at the top are in scale.

References

Menter, F. R. (2003). Ten years of industrial experience with the SST turbulence model. *Turbulence, Heat and Mass Transfer*, *4*, 625–632.